Active and Passive Mechanisms of [Fluorine-18] Fluorodeoxyglucose Uptake by Proliferating and Prenecrotic Cancer Cells In Vivo: A Microautoradiographic Study

Roko Kubota, Kazuo Kubota, Susumu Yamada, Masao Tada, Tatsuo Ido and Nobuaki Tamahashi

Departments of Nuclear Medicine and Radiology and Pharmacology, Institute for Aging, Development and Cancer; and Cyclotron and Radioisotope Center, Tohoku University; and Clusterecore Institute of Biology, Sendai, Japan

In this study, [^{18}F]FDG uptake mechanisms were investigated in neoplastic cells during cell proliferation and cell death. **Methods:** Detailed analysis was performed on mouse tumor models of different growth rates using [^{18}F]FDG, [6-^{3}H]thymidine [^{3}H]Thd (a precursor of DNA synthesis) and [^{125}I]bovine serum albumin ([^{125}I]BSA) (a marker of diffusion) with autoradiographic and histopathologic techniques and electron microscopy. **Results:** The three compounds, [^{18}F]FDG, [^{3}H]Thd and [^{125}I]BSA, showed different heterogeneous patterns of distribution within tumor tissue sections in neoplastic and non-neoplastic cellular elements. The uptake of [^{18}F]FDG by prenecrotic (or necrobiotic) tumor cells surrounding focal necrotic cell debris was 1.5 to 2.3 times higher than that of viable tumor cells. Prenecrotic cells did not retain trapped [^{18}F]FDG; therefore, the uptake was considered to be nonmetabolic. Inconspicuous cell membrane, vesicular cytoplasmic organelles and condensed nuclear chromatin were remarkable findings in the prenecrotic cells. A comparison of viable tumor cells in tumors undergoing different growth rates showed that the ratio of [^{18}F]FDG uptake was similar to that of [^{3}H]Thd uptake in each S-phase cell. Fluorine-18-FDG showed a cell cycle dependency, with a higher uptake observed in cells in G_0/G_1 and G_2 phases of the cell cycle compared with the S and M phases. **Conclusion:** A passive mechanism of [^{18}F]FDG uptake may exist in the necrobiotic/prenecrotic or hypoxic/anoxic cells in tumors. However, the discordance of [^{18}F]FDG and [^{3}H]Thd uptake may be the result of the different cell cycle dependency of tracer uptake in the same tumor.

Key Words: [fluorine-18] fluorodeoxyglucose; cancer; autoradiography; cell cycle; tritiated thymidine

J Nucl Med 1994; 35:1067–1075

A recent in vivo autoradiographic study (*1*) demonstrated that uptake of [^{18}F]fluorodeoxyglucose ([^{18}F]FDG), a radiotracer used for tumor detection by PET (*2–5*), per unit area by macrophages and young granulation tissue was higher than uptake by viable tumor cells. Histologically, tumors are composed of both neoplastic cells and nonneoplastic elements, such as tumor-associated macrophages (*6,7*). The uptake of [^{18}F]FDG by the whole tumor is, therefore, considered to be the result of uptake by both neoplastic and nonneoplastic cellular components (*8*). The [^{18}F]FDG uptake pattern of each cellular component in a particular tumor tissue changes with time (*9*). For example, macrophages show an increasing pattern of uptake. The uptake in tumor cells and young granulation tissue reaches a plateau, and the focal necrotic area shows a peak followed by a decreasing pattern, up to 120 min after injection (*9*). The mechanism of accumulation of [^{18}F]FDG into neoplastic cells (*10–13*) and into tumor-associated macrophages and granulation tissues (*7*) is believed to be caused by an enhanced rate of glucose utilization. However, the high concentration of the tracer in an area of focal necrosis that is devoid of phagocytes is difficult to explain by the process of active glucose utilization.

In this study, a relationship was demonstrated between DNA synthetic activity and [^{18}F]FDG uptake in in vivo tumor models of different growth rates. The cell-cycle dependency of [^{18}F]FDG uptake was also illustrated in each tumor by using autoradiographic, histopathologic and electron microscopic techniques. The mechanism of [^{18}F]FDG uptake observed in prenecrotic (necrobiotic or biologically hypoxic) cells in areas with focal necrosis is also discussed.

MATERIALS AND METHODS

Animal Models

The experimental protocol was approved by the Laboratory Animal Care and Use Committee of Tohoku University. Ten-wk-old C3H/He female mice were subcutaneously injected with 0.1 ml of a suspension of 10^7 syngeneic FM3A mammary carcinoma cells on the left thigh and 10^6 syngeneic MH134 hepatoma cells on the right thigh. Preliminary experiments indicated that the rate of growth of MH134 was faster than that of FM3A. Therefore, to prepare tumor models of the same age and of equal volumes for tracer experiments, a smaller number of inoculated tumor cells

Received June 29, 1993; revision accepted Mar. 1, 1994.

For correspondence or reprints contact: Roko Kubota, PhD, Department of Nuclear Medicine and Radiology, Institute for Aging, Development and Cancer, Tohoku University, 4-1 Seiryo-cho, Aoba-ku, Sendai 980, Japan.

were used in the MH134 model. The growth curves of such tumors were described in detail elsewhere (*9*). Tracer experiments were performed 10 days after transplantation when the volume doubling time was 1.3 days for MH134 and 4.9 days for FM3A. The tumor volumes of both models were the same (FM3A = 438 ± 82 mm^3; MH134 = 450 ± 86 mm^3). The mice were fasted for 12 hr before the experiment but were provided with water ad libitum.

Double-Tracer Macroautoradiography with [^{18}F]FDG and Tritiated Thymidine or Iodine-125-Labeled Bovine Serum Albumin

Three C3H mice with FM3A and MH134 tumors received an intravenous injection of a mixture of 200 μCi (7.4 MBq) of [^{18}F]FDG and 30 μCi (1.11 MBq) of [6-^{3}H]thymidine ([^{3}H]Thd, Amersham International, Buckinghamshire, UK) in 0.2 ml. Three other mice were given, through the same route, a mixture of 200 μCi (7.40 MBq) of [^{18}F]FDG and 10 μCi (0.37 MBq) of [^{125}I]-bovine serum albumin ([^{125}I]BSA, New England Nuclear, Wilmington, Delaware) in 0.2 ml. All animals were killed 1 hr after the injection of the tracer. The tumors were quickly dissected and prepared for frozen sectioning, as reported previously (*5*). Several 3.5-μm thick sections were mounted on clean glass slides, air dried and directly underwent contact with autoradiography (ARG) film (MARG ^{3}H type, Konica, Tokyo, Japan) for 2 hr to produce [^{18}F]FDG images. After the decay of ^{18}F radioactivity, the same sections underwent contact 3 days later with separate films for 8 wk to produce [^{3}H]Thd images and for 3 wk to produce [^{125}I]BSA images. All sections were stained with hematoxylin and eosin (H & E) after exposure. There was no cross-talk of ^{3}H on the ^{18}F autoradiogram, as measured by a precision densitometer. The film response curves for ^{18}F and ^{3}H were reported previously (*9*).

Micro-ARG

Seven C3H mice bearing both FM3A and MH134 tumors were intravenously injected with a mixture of 1 mCi (37 MBq) of [^{18}F]FDG and 30 μCi (1.11 MBq) of [^{3}H]Thd in 0.2 ml. In addition, intravenous injection of a mixture of 1 mCi (37 MBq) of [^{18}F]FDG and 10 μCi (0.37 MBq) of [^{125}I]BSA in 0.2 ml was performed in five mice. All animals were killed 1 hr after injection of the tracer. The tumors were quickly dissected and prepared for frozen sectioning, as described earlier. Several 3.5-μm thick sections were processed for micro-ARG by using NTB2 nuclear emulsion (*5*) just after tracer experiments for [^{18}F]FDG and, 3 days later, for [^{3}H]Thd and [^{125}I]BSA, respectively. After 4-hr, 2-wk and 3-wk exposure for [^{18}F]FDG, [^{3}H]Thd and [^{125}I]BSA, respectively, the sections were developed, fixed and stained with H & E. Nonradioactive tumor sections were treated similarly for chemographic control. Silver grain counts were performed in the various tumor cell regions under a transmitted light bright-field microscope. The background level was subtracted from the relevant data. Comparisons between two sets of data were performed using a Student's t-test.

The relationship between the number of grains and ^{18}F or ^{3}H radioactivity was determined and reported previously (*5,9*). The linear relationship between grain numbers and the corresponding radioactivity was previously determined for each tracer. In ^{125}I micro-ARG, the linear relationship between grain numbers and radioactivity was also reported by Schnitzer et al. (*14*). These early studies validated grain counting as a method for the quantification of micro-ARG for [^{18}F]FDG, [^{3}H]Thd and [^{125}I]BSA. Cells in the DNA synthetic phase (S phase) of the cell cycle were labeled with [^{3}H]Thd. The quantitative characteristics of [^{3}H]Thd micro-ARG have been determined over the last several years and established as a marker of de novo DNA synthesis (*15–18*).

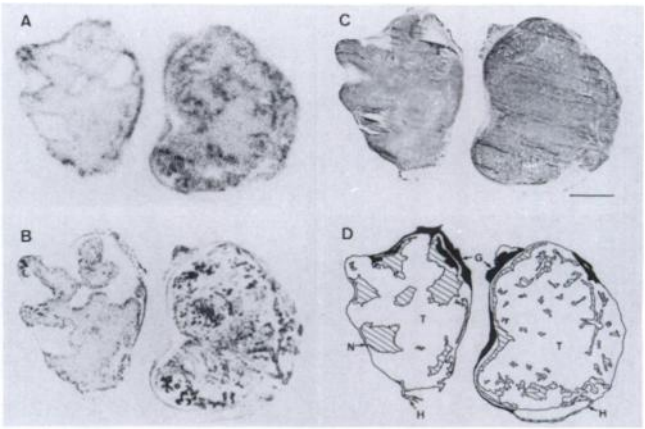

FIGURE 1. A combination of double-tracer macroautoradiograms and microscopy. Images of [^{18}F]FDG distribution (A) and [^{3}H]Thd (B) and a photomicrograph of the specimen (C), which produced the autoradiograms and the illustration of the micrograph (D). Left = FM3A; right = MH134; T = tumor cells; G = granulation tissue; N = necrosis; H = host normal tissue. Scale bar = 2 mm.

Double-Tracer Micro-ARG with [^{18}F]FDG and [^{3}H]Thd

Sections with [^{18}F]FDG and [^{3}H]Thd were also used for a double-tracer micro-ARG, as reported previously (*19*). After 3 days, following [^{18}F]FDG micro-ARG, the second ARG was performed by using an ET2F stripping film (Fuji, Tokyo, Japan). Under a safety light, slides containing tissue sections and the first autoradiogram were covered with ET2F stripping film. Film-coated slides were exposed for 3 wk at a later stage, followed by development, fixation and staining with H & E.

The [^{3}H]Thd-labeled cells were identified by focusing a transmitted light bright-field microscope on the upper emulsion layer of ET2F film. The tumor cells were divided into S-phase and non-S-phase cells by [^{3}H]Thd labeling. The grain counts of [^{18}F]FDG autoradiograms were obtained by focusing the microscope on the lower emulsion layer (NTB2) using a micrometer. The maximum cross-talk of ^{3}H on the ^{18}F microautoradiogram was small (0.8%) and accordingly ignored.

Electron Microscopic Examination

Three tumor pairs of MH134 and FM3A were quickly dissected 10 days after transplantation, trimmed and fixed in a conventional 2.5% cacodylate-buffered glutaraldehyde, postfixed in 1% buffered osmium tetroxide, dehydrated and embedded in Epon 812 (Taab Laboratories Equipment, Berkshire, UK). Ultrathin sections (700 Å) were stained with uranyl acetate-lead citrate. The areas between focal necrotic cell debris and viable tumor cells were examined with an electron microscope.

RESULTS

DNA Synthesis and [^{18}F]FDG Uptake

Figure 1A and B shows a combination of double-tracer autoradiograms of a section of both MH134 and FM3A tumors 1 hr after the injection of a mixture of [^{18}F]FDG and [^{3}H]Thd. Both tracers showed different patterns of heterogeneous grain density distribution within the tissue sections, including neoplastic and nonneoplastic cellular ele-

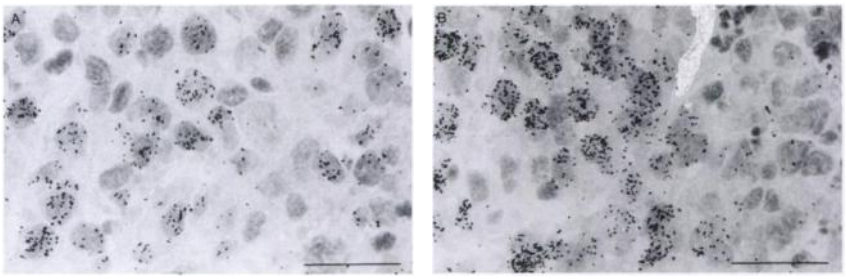

FIGURE 2. Microautoradiograms of a pulse-labeling with [^{3}H]Thd. (A) FM3A. (B) MH134. Labeled cells were in the S phase of cell cycle 1 hr before when the tracer was injected. Notice the large number of grains in labeled MH134 cells compared with FM3A. Also note the smaller MH134 cell size compared with those of FM3A. Scale bar = 30 μm.

ments. MH134 showed a higher and more accentuated grain density distribution of both tracers than did FM3A. The [^{18}F]FDG autoradiogram showed the highest density along the tumor rim and edges of extensive necrosis. It also showed accentuated dense spots in areas of focal necrosis within the tumor, corresponding to the translucent area on the [^{3}H]Thd autoradiogram. Dense areas on the [^{3}H]Thd autoradiogram corresponded with proliferating cell regions, as determined by 1-hr pulse labeling. MH134 showed numerous focal areas of necrosis, but these areas were smaller in size than those in FM3A; FM3A showed larger areas of necrosis.

Cells labeled with [^{3}H]Thd were in the S phase of the cell cycle when the tracer was injected (Fig. 2). By micro-ARG, the distribution of [^{3}H]Thd-labeled cells in MH134 tended to be limited around the blood vessels (Fig. 2B); labeled cells in FM3A distributed semihomogeneously in neoplastic cells (Fig. 2A), as also observed by macro-ARG in Figure 1B. The number of grains by [^{3}H]Thd in each labeled cell was greater in MH134 than in FM3A.

Table 1 summarizes the profile of FM3A and MH134 tumor cells in the tumor tissue 1 hr after a simultaneous injection of tracers. The [^{3}H]Thd labeling indices, representing the proportion of S-phase cells in viable tumor cells, were the same in FM3A and MH134, even though the pattern of labeled cell distribution was different in the two tumors. The cell density and [^{3}H]Thd grain numbers per S-phase cell and unit area of S-phase cell and the [^{18}F]FDG grain numbers in a unit area of viable tumor cells, including all phases of cells, were higher in MH134 than in FM3A ($p < 0.05$, $p < 0.001$ and $p < 0.001$, respectively). The MH134/FM3A ratio of [^{3}H]Thd grain numbers per unit area of S-phase cells (1.84) was not different from that of [^{18}F]FDG grain numbers per unit area of viable tumor cells (1.89).

[Fluorine-18]FDG Uptake During a Cell Cycle

Figure 3 shows two pairs of double-tracer microautoradiograms in viable tumor cell layers of FM3A and MH134, 1 hr after injecting a mixture of [^{18}F]FDG and [^{3}H]Thd. It is possible to compare the distribution of S- and non-S-phase cells visually and the grain level of [^{18}F]FDG on each cell in the same area. The S-phase cells seemed to have less grain density than did the non-S-phase cells. Table 2 represents the cellular [^{18}F]FDG uptake by cells in S phase, mitosis (late metaphase to anaphase) and non-S/non-M phase selected by [^{3}H]Thd labeling and mitosis. The

TABLE 1
Microautoradiography-Derived Quantitative Results of DNA Synthesis Activity and [Fluorine-18]FDG Uptake*

		[^{3}H]Thd†			[^{18}F]FDG‡	
	Cell density† (cells/10^4 μm^2)	LI (%)	Grains/ Labeled cell	Grains/100 μm^2/ labeled cell	Grains/100 μm^2/ viable cell	DUR
FM3A	48.9 ± 5.4§	31.8 ± 10.4	30.13 ± 17.36¶	14.73 ± 8.49¶ (1.00)	9.78 ± 2.86¶ (1.00)	2.21 ± 0.26¶ (1.00)
MH134	57.4 ± 11.0	31.9 ± 14.9	47.28 ± 21.34	27.14 ± 12.25 (1.84)	18.51 ± 5.74 (1.89)	3.67 ± 0.17 (1.66)

*Mean ± s.d.
†Fifteen sections of seven tumors each, total of 1556 cells for FM3A and 1826 cells for MH134, were analyzed. Seventy-seven labeled cells for FM3A and 76 labeled cells for MH134 were counted.
‡Fourteen sections of seven tumors each and four microgrid areas for each section were analyzed for grain counts, with five tumors each for DUR.
§$p < 0.05$.
¶$p < 0.001$ compared with MH134.

$$DUR = \frac{\text{tissue counts/tissue weight}}{\text{injected dose counts/body weight}}$$

LI = labeling index; i.e., percentage of labeled cells to total tumor cells; DUR = differential uptake ratio, see below; parentheses = ratio to FM3A.

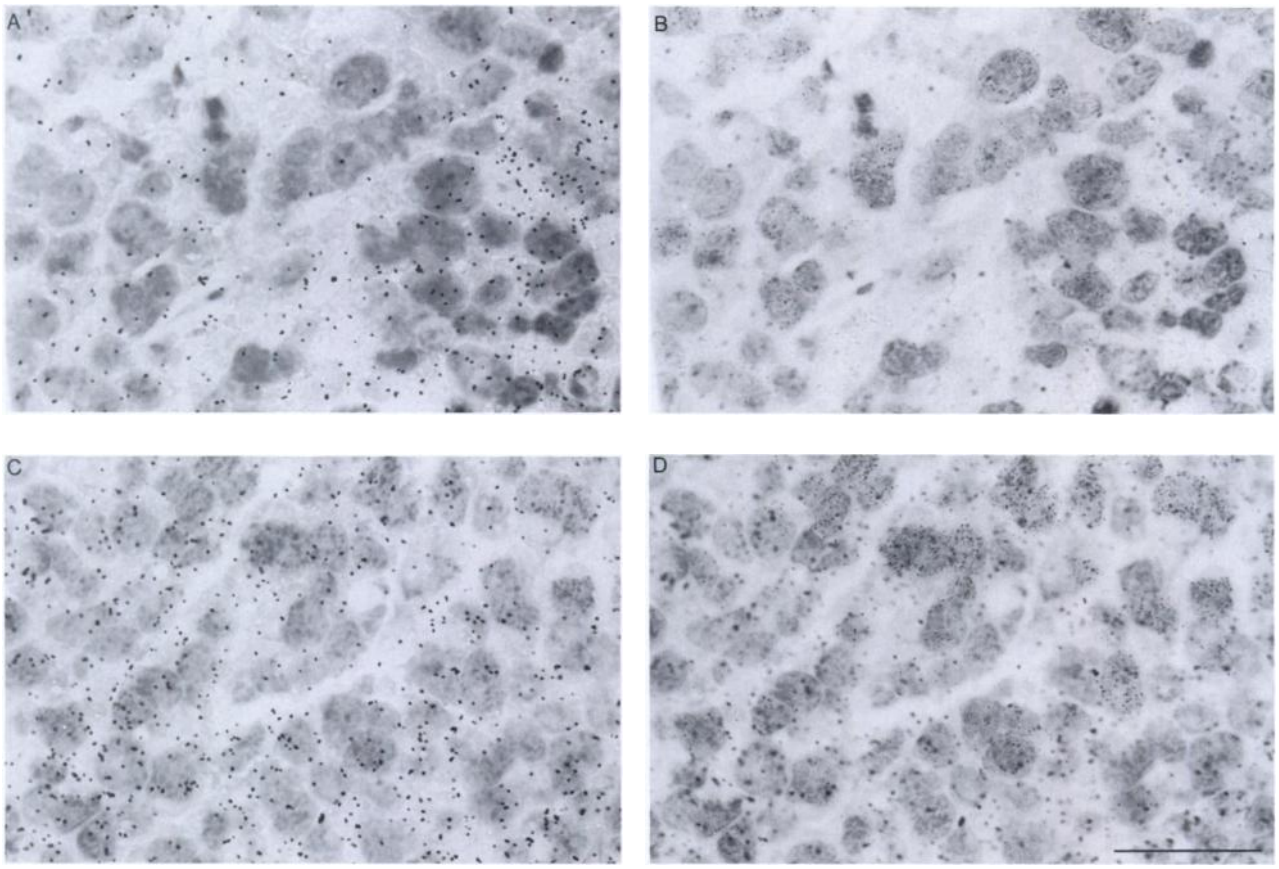

FIGURE 3. Two pairs of double-tracer microautoradiograms with [^{18}F]FDG and [^{3}H]Thd. (A) [^{18}F]FDG in FM3A. (B) [^{3}H]Thd in FM3A. (C) [^{18}F]FDG in MH134. (D) [^{3}H]Thd in MH134. The [^{18}F]FDG autoradiograms were focused on the lower emulsion (NTB2) layer. The [^{3}H]Thd autoradiograms were focused on the upper emulsion (ET2F stripping film) layer within the same area of [^{18}F]FDG autoradiograms. Scale bar = 30 μm, as indicated on (D).

[^{18}F]FDG uptake was significantly ($p < 0.001$) higher in non-S-/non-M-phase cells than in M- and S-phase cells in each tumor model.

[Fluorine-18]FDG Uptake by Damaged Tumor Cells

Figures 4A and B show a combination of double-tracer autoradiograms and a photomicrogram of a section of MH134 and FM3A tumors (Fig. 4C) 1 hr after injection of a mixture of [^{18}F]FDG and [^{125}I]BSA. These autoradiograms showed that the latter grains were dense in large necrotic areas and in the intact host tissue. By contrast, [^{18}F]FDG grain densities were low in the corresponding regions (see arrows), probably representing a smaller diffusion of [^{18}F]FDG into extensive necrotic areas. Some of the marked dense spots (see arrowheads) in the viable tumor tissue were observed only in [^{18}F]FDG autoradiograms. Grain densities in all areas of ^{18}F and ^{125}I autoradiograms were higher in MH134 than in FM3A tumors. Although [^{18}F]FDG grain density in extensive necrosis was low in the macroautoradiogram, a small amount of homo-

TABLE 2
Grain Counts Data on [Fluorine-18]FDG Uptake in Cells*†

	S phase	M phase	non-S/non-M phase
FM3A‡	3.37 ± 0.71 (n = 91)	1.84 ± 0.80 (n = 13)¶	5.48 ± 1.12 (n = 376)
MH134§	5.97 ± 2.10 (n = 101)	1.53 ± 1.33 (n = 9)	8.70 ± 1.79 (n = 348)

*Mean ± s.d. Grain numbers per cell. n = number of cells counted.

†S phase: tritiated thymidine-labeled cells, M phase: histologically confirmed mitotic cells in late metaphase to anaphase, non-S/non-M phase: cells except S and M phase. Grains grew larger by double development during the process of double-tracer microautoradiography; therefore, the number of grains resolved became lower than, but was correlated with, the original microautoradiography.

‡and §: $p < 0.001$ among the three phases in each tumor.

‡ versus §: $p < 0.001$ in S and non-S/non-M phases.

¶Not significant in M phases of the two tumors.

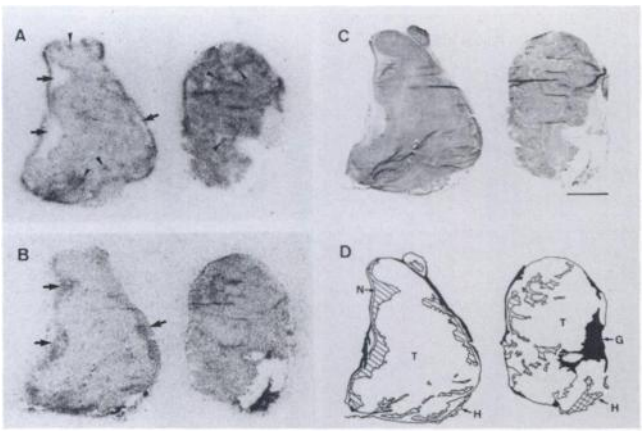

FIGURE 4. A combination of double-tracer macroautoradiograms and microscopy. Images of [^{18}F]FDG distribution (A) and [^{125}I]BSA (B) and a photomicrograph of the specimen (C), which produced autoradiograms and the illustration of the micrograms (D). Left = FM3A; right = MH134. Notice the small [^{18}F]FDG uptake in extensive necrotic areas (arrows, A) and high [^{125}I]BSA uptake in the same areas (arrows, B). Some of the marked dense spots were observed only in the [^{18}F]FDG autoradiogram (arrowheads, A). The host tissue in MH134 includes a mammary gland. The definitions are as in Figure 1. Scale bar = 2 mm.

geneous grain distribution, which was almost equal to the background level, was found in areas with extensive necrosis without phagocytic infiltration in [^{18}F]FDG microautoradiograms (Fig. 5A). Focal necrotic areas observed as marked dense spots in [^{18}F]FDG autoradiograms (see arrowheads in Fig. 4A) were composed of focal necrotic cell debris surrounded by "healthy-looking" tumor cells. By micro-ARG, high [^{18}F]FDG uptake by healthy tumor cells was observed in the same region (Fig. 5C). Electron microscopy revealed damaged cell membranes and intracellular components in healthy tumor cells of the same histologic region (Fig. 6B). These cells were termed prenecroticcells (or necrobiotic).

Typical microautoradiograms of [^{18}F]FDG and [^{125}I]BSA from the extensive and focal necrotic areas are shown in Figure 5. Table 3 summarizes the micro-ARG quantification of grain numbers in necrotic areas and viable tumor cells. The uptake of [^{125}I]BSA in extensive necrotic areas was high and similar to that in focal necrotic cell debris (Fig. 5). However, the uptake of the same tracer in viable and prenecrotic tumor cells around cell debris (Fig.

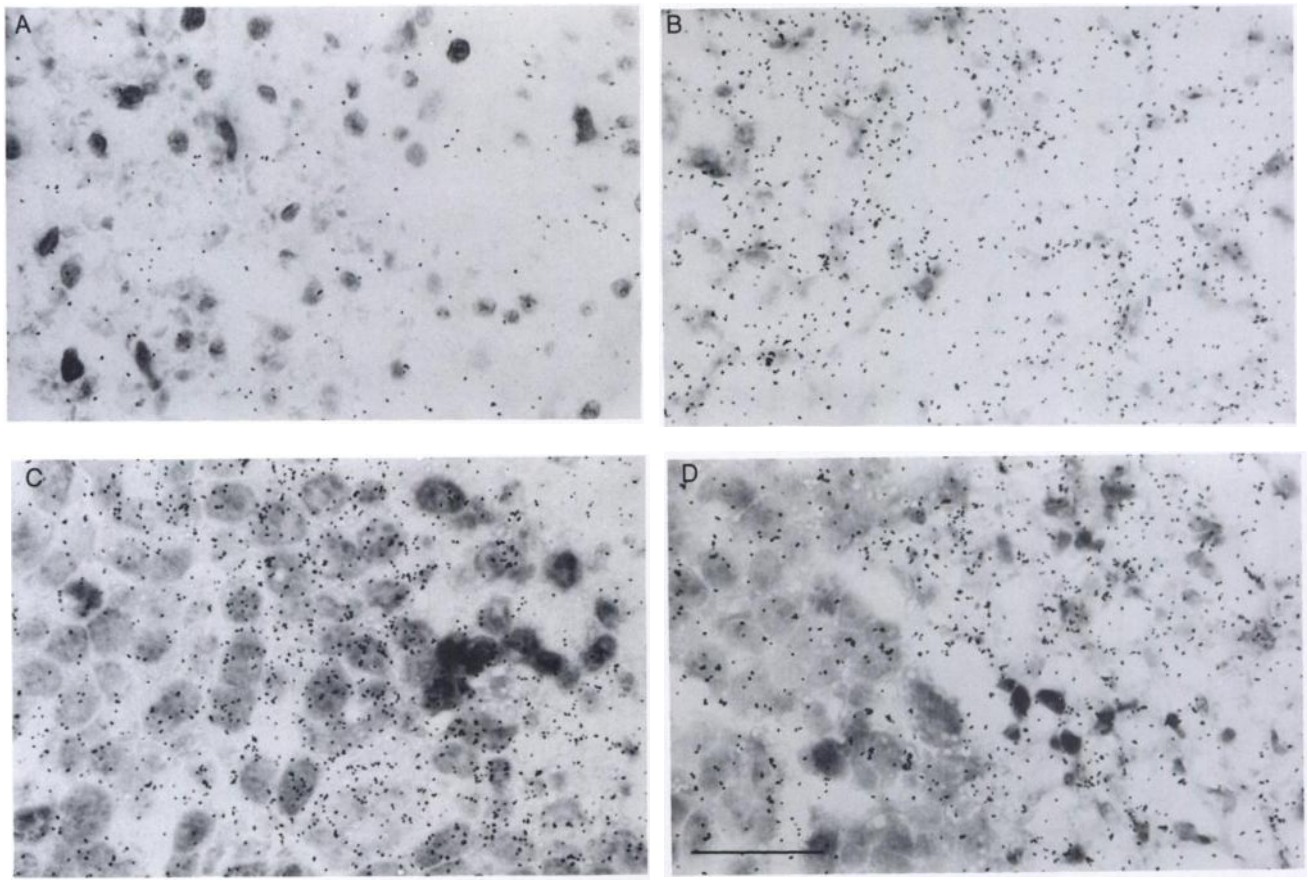

FIGURE 5. Microautoradiograms histologically corresponding to [^{18}F]FDG and [^{125}I]BSA in MH134. [^{18}F]FDG (A) and [^{125}I]BSA (B) in an extensive necrotic area. [^{18}F]FDG (C) and [^{125}I]BSA (D) in a focal necrotic area. Focal necrotic areas were composed of focal necrotic cell debris and surrounding prenecrotic tumor cells. The [^{18}F]FDG grains were located more on prenecrotic tumor cells. The [^{125}I]BSA grain densities on the extensive necrotic area and on focal necrotic cell debris were similar and markedly greater than those on tumor cells. Notice similar [^{125}I]BSA grain densities on prenecrotic tumor cells and proliferating tumor cells. Scale bar = 30 μm, as indicated on D.

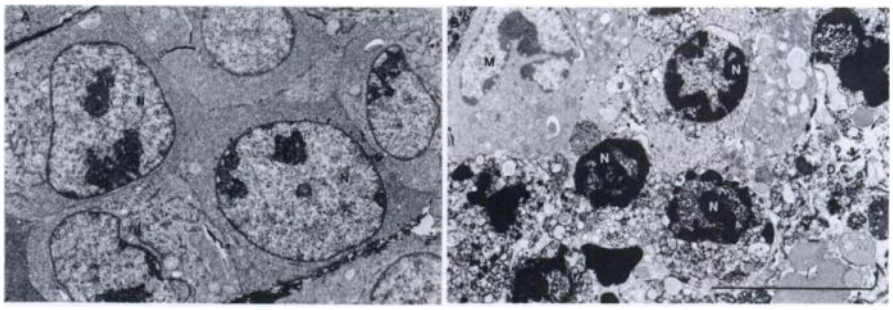

FIGURE 6. Electron microscopy of intact tumor cells (A) and prenecrotic tumor cells (B). Viable tumor cells are rich in free ribosomes and have small numbers of organelles, such as mitochondria and granular endoplasmic reticulum. In prenecrotic tumor cells, nuclear chromatin is markedly condensed or pyknotic, and vesicular structures fill the cytoplasm. N = tumor cell nucleus; M = macrophage; D = cell debris. Bar = 10 μm, as indicated on B.

5) was significantly low ($p < 0.001$) in both FM3A and MH134 tumors. On the other hand, [^{18}F]FDG uptake in extensive necrotic areas and cell debris was very low, but that in prenecrotic and viable tumor cells was 8.7 to 9.9 and 4.2 to 6.3 times higher ($p < 0.001$) than that in areas with extensive necrosis.

Figure 6 shows a pair of electron micrographs of MH134 tumor cells: one obtained in the proliferative area and the other in the prenecrotic area surrounding the focal necrotic cell debris. Inconspicuous cell membrane, vesicular cytoplasmic organelle and condensed nuclear chromatin characterized the cells found in the prenecrotic area. These cellular features represent morphologic signs, ranging from irreversible cell damage to cell death. These cells did not show noticeable histologic changes in H & E-stained autoradiograms under light microscopy.

DISCUSSION

Decreased tissue oxygenation and reduced blood flow are thought to be the underlying mechanisms of prenecrosis of tumor cells (*20*). Hypoxic cells have been recently reported to have a high FDG uptake, as demonstrated in vitro culture studies by Wahl et al. (*21,22*). In addition, an ARG study using xenografts of a human tumor into nude mice with a negligible host immune reaction revealed a high 2-deoxyglucose (2-DG) uptake by healthy-looking cancer cells (under the light microscope) surrounding a small necrotic area (*23*). Irregular FDG uptake by tumor cells after radiotherapy was also reported (*24*). Furthermore, in a recent in vitro study of human ovarian carcinomatous cells, FDG uptake and that of methionine and thymidine increased following irradiation with 30 Gy of ^{60}Co. Increased uptake occurred in spite of a decline in viable cell numbers (*25*). Finally, in recent clinical FDG-PET studies, the glucose uptake ratio of brain tumors increased after radiotherapy (*26*) and chemotherapy (*27*) before declining. These studies indicate that the treatment of malignant tumors may render some cells prenecrotic or in the process of dying. In addition, anoxic or ischemic injured cardiac myocytes also showed an accumulation of ^{99m}Tc-gluconate (*28,29*), ^{99m}Tc-glucarate or [^{3}H]DG (*29*). Thus, the concept of prenecrosis is based on the histopathologic features of cells; that of hypoxic/anoxic cell injury is based on cellular biology. A characteristic change in FDG/2-DG uptake and other tracers by prenecrotic/hypoxic cells may be a common feature following the commencement of irreversible cell death. Unknown but common cellular mechanisms of tracer uptake that are different from energy-coupling active transport and glucose utilization may exist in cells after the loss of viability.

It has been demonstrated that, in a degenerative process in which cells were able to recover, the loss of viability was the consequence of failed energy metabolism, as assessed by 2-DG uptake (*31*). Furthermore, a positive correlation

TABLE 3
Difference Between Diffusion/Permeation by Iodine-125-Bovine Serum Albumin and [Fluorine-18] FDG Uptake*

	FM3A		MH134	
	[^{125}I]BSA	[^{18}F]FDG	[^{125}I]BSA	[^{18}F]FDG
Extensive necrosis	20.74 ± 6.68†	2.31 ± 1.68‡	27.13 ± 4.11†	2.96 ± 1.57§
Focal necrotic area				
Cell debris	21.62 ± 6.43†	3.61 ± 1.33‡	27.98 ± 4.11†	4.36 ± 2.03§
Prenecrotic cells	8.15 ± 1.68¶	20.08 ± 5.29**	13.43 ± 2.23¶	29.33 ± 6.75**
Viable tumor cells	6.85 ± 2.93¶	9.78 ± 2.86**	12.35 ± 3.59¶	18.51 ± 5.74**

*Mean ± s.d. of grain numbers per 100 μm^2. Thirteen sections of five tumors each for [^{125}I]BSA and 14 sections of seven tumors each for [^{18}F]FDG were analyzed. Four microgrid areas for each region were counted and averaged as a value of the section.

† versus ¶, ‡ versus **, § versus **: $p < 0.001$ in each tumor.

† and ¶: Not significant in each pair in each tumor.

**$p < 0.001$ in each pair in each tumor.

$^{\ddagger}p < 0.05$ and $^{\S}p < 0.1$ in each pair.

between the cellular adenosine triphosphate (ATP) level and [^{18}F]FDG uptake was also reported in cultured neoplastic cells (*32*). The results of other studies indicate that a marked decrease in cellular ATP level precedes the changes in cell membrane permeability because the integrity of the membrane is dependent on an adequate energy level (*28,29,33*). Cell membrane dysfunction, which is caused by diminished energy level, is a primary event heralding the initiation of irreversible cell death (*32*). This phenomenon leads to a cascade of events (*33*). The first process involves a gradual increase in cell membrane permeability, characterized by a decrease in the trypan blue exclusion frequency and leakage of cytoplasmic enzymes. This is followed by an intracellular accumulation of tracers (*28–30*), cell swelling and death. In this regard, reoxygenation after the initiation of cell death may only temporarily halt the process of cell death, the cells usually disintegrate in spite of an increased oxygen supply (*28*). Radiation-induced cell injury causing giant cell formation is evidence of the dying (prenecrotic) cells (*34*), regardless of the supplies of oxygen. Thus, high [^{18}F]FDG uptake by necrobiotic cells surrounding focal necrotic cell debris and by radiation-injured giant cells (*25*) is believed to represent this process, causing cell membrane dysfunction and failure of mechanisms controlling membrane permeability and leading to irreversible progression toward death rather than transient proliferation (*36*). A schematic diagram of the histologic and biologic processes and [^{18}F]FDG uptake is shown in Figure 7. It was previously demonstrated that accumulated [^{18}F]FDG in prenecrotic cells was not phosphorylated because the uptake of these cells showed a clearance pattern after reaching a peak 30 min after injection (*9*). By contrast, other cellular elements of tumor tissue showed an increasing or plateau pattern 60 min after injection, suggesting phosphorylated trapping of the accumulated tracer in the cell. Based on these results, it was proposed that the mechanism of [^{18}F]FDG uptake by prenecrotic cells may be different from ATP-coupling phosphorylation because it is unlikely that dying cells retain a high level of ATP for metabolism or that they are metabolically more active than the viable cells adjacent to blood vessels.

Studies by Shields et al. (*37–39*) recently demonstrated a discordance in the uptake and retention of [^{11}C]Thd and [^{18}F]FDG. These investigators described a heterogeneous uptake of these two tracers, e.g., areas with the highest uptake of [^{11}C]Thd and [^{18}F]FDG were different, and no correlation was seen. These results are consistent with the ARG image profile of mouse tumors reported here. In addition to the heterogeneous cellular components of tumor tissues, a difference in cell-cycle dependency between [^{18}F]FDG uptake (higher in cells in gap phases) and [^{3}H]Thd uptake (higher in cells in S phase) supports these image profiles.

In this regard, a recent in vitro study examining human adenocarcinomatous cells (*39*) reported that the uptake of [^{3}H]FDG did not relate with the proliferative activity of

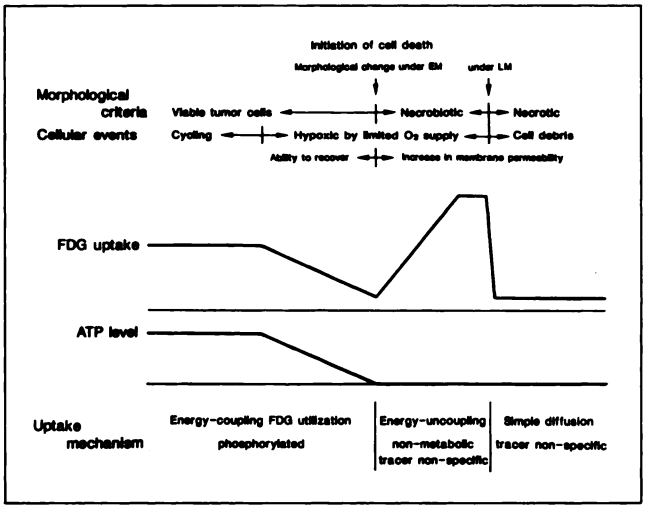

FIGURE 7. A schematic diagram of the proposed [^{18}F]FDG uptake by tumor cells.

cancer cells. The in vivo finding of cell-cycle dependency of [^{18}F]FDG uptake in the current study also supports the results of this earlier study. Higher levels of FDG accumulated in a group of cells with greater gap phase cells (a plateau phase in culture); [^{3}H]Thd accumulated to a lesser degree in the same group of cells. These findings were reversed in a group of cells with a greater number of S-phase cells (a lag phase in culture). These results suggested that [^{18}F]FDG uptake may not be related to [^{3}H]Thd uptake in viable tumor cells. This conclusion, however, may not be applicable to tumors with different growth rates. The MH134/FM3A ratio of [^{18}F]FDG uptake by viable tumor cells was comparable with that of [^{3}H]Thd uptake by S-phase cells in the same unit area. In other words, viable tumor cells with a faster growth rate showed a higher [^{18}F]FDG uptake that was comparable to the ratio of the DNA synthetic rate. Enzymatically, tumors with faster growth rates contain a higher level of glucose hexokinase (*41*). Thus, a correlation between [^{18}F]FDG and [^{3}H]Thd uptake may exist when comparing tumors with different growth rates but not in a serial follow-up study of the same tumor.

The principal process providing energy for mitosis was previously thought to be glucose oxidation. The rate of glucose oxidation was related to the activation of hexose monophosphate shunt enzymes (*42,43*). These early studies also proposed a concept of cell-cycle dependency to explain the rate of glucose oxidation, which increased during the period between divisions and decreased during mitoses. Recent studies using flow-cytometric analysis enabled a precise identification of the various events occurring during each cell cycle phase rather than only during mitosis. These studies revealed that stimulation of glucose transport is one of the early events occurring prior to the reinitiation of DNA synthesis in quiescent cells (*44,45*). In proliferative thymocytes, a concomitant increase in the rate of DNA synthesis and glycolysis was observed. How-

ever, the maximal increment in the glycolytic rate preceded that of DNA synthesis (*46*). Insulin binding sites were the greatest in G_2+M phase followed by G_0/G_1 and the lowest in S (*47*). These studies support the results found here that higher [^{18}F]FDG uptake was observed in cells in non-S/non-M (late metaphase to anaphase) phases; therefore, the G_0/G_1 and G_2/M (prophase, prometaphase and telophase). The cell cycle is a set of events responsible for the duplication of the cell (*48*). Cycling cells may consume glucose for the S phase during the G_0/G_1 phase and for M phase during the G_2 phase of the cell cycle.

CONCLUSION

Prenecrotic (necrobiotic) cells surrounding focal necrotic cell debris were histopathologically in the initial phase of irreversible cell death and were considered to be biologically hypoxic. The accumulation of [^{18}F]FDG in these cells occurred passively as a result of an altered permeability of injured cell membranes.

The tracers [^{18}F]FDG, [^{3}H]Thd and [^{125}I]BSA showed different heterogeneous patterns of distribution within the tumor tissue sections. The MH134/FM3A ratio of [^{18}F]FDG uptake by viable tumor cells corresponded to that of [^{3}H]Thd uptake by S-phase cells. This finding indicated that viable tumor cells with a faster growth rate have a higher [^{18}F]FDG uptake, which is comparable to the ratio of the DNA synthetic rate. The [^{18}F]FDG uptake in viable tumor cells seemed to be a marker of proliferative activity in a comparative study. In each tumor, [^{18}F]FDG uptake by viable tumor cells showed a cell-cycle dependency with an increased uptake in those cells in G_0/G_1 and G_2 phases. Cycling cells may consume glucose for DNA synthesis and mitotic division when they are in gap phases. This phenomenon may induce a discordance between [^{18}F]FDG and [^{3}H]Thd uptake when studying the same tumor.

ACKNOWLEDGMENTS

The authors thank Dr. Prantika Som, Brookhaven National Laboratory (Upton, NY) for advice; the staffs of the Cyclotron and Radioisotope Center, Tohoku University for their cooperation; the staff of Clusterecore Institute of Biology for their excellent histological assistance; and Mr. Y. Sugawara for photography. This work was supported by a grant-in-aid (03454277 and 04557047) from the Ministry of Education, Science and Culture, Japan.

REFERENCES

1. Kubota R, Yamada S, Kubota K, et al. Intratumoral distribution of fluorine-18-fluorodeoxyglucose in vivo: high accumulation in macrophages and granulation tissues studied by microautoradiography. *J Nucl Med* 1992;33:1972–1980.
2. Som P, Atkins HL, Bandoypadhyay D, et al. A fluorinated glucose analog, 2-fluoro-2-deoxy-D-glucose (F-18): non-toxic tracer for rapid tumor detection. *J Nucl Med* 1980;21:670–675.
3. Larson SM, Weiden PL, Grunbaum Z, et al. Positron imaging feasibility studies. II. Characteristics of 2-deoxyglucose uptake in rodent and canine neoplasms: concise communication. *J Nucl Med* 1981;22:875–879.
4. Di Chiro G, DeLaPaz RL, Brooks RA, et al. Glucose utilization of cerebral gliomas measured by [^{18}F]-fluoro-deoxyglucose and positron emission tomography. *Neurology* 1982;32:1323–1329.
5. Yonekura Y, Benua RS, Brill AB, et al. Increased accumulation of 2-deoxy-2-([^{18}F)fluoro-D-glucose in liver metastases from colon carcinoma. *J Nucl Med* 1982;23:1133–1137.
6. Steele RJC, Brown M, Eremin O. Characterisation of macrophages infiltrating human mammary carcinomas. *Br J Cancer* 1985;51:135–138.
7. Graves DT, Valente AJ. Monocyte chemotactic proteins from human tumor cells. *Biochem Pharmacol* 1991;41:333–337.
8. Kubota K, Kubota R, Yamada S. FDG accumulation in tumor tissue (Editorial). *J Nucl Med* 1993;34:419–421.
9. Kubota R, Kubota K, Yamada S, et al. Microautoradiographic study for the differentiation of intratumoral macrophages, granulation tissues and cancer cells by the dynamics of fluorine-18-fluoro-deoxyglucose uptake. *J Nucl Med* 1994;35:104–112.
10. MacKeehan WL. Glycolysis, glutaminolysis and cell proliferation. *Cell Biol Int Rep* 1982;6:635–650.
11. Sweeney MJ, Ashmore J, Morris HP, Weber G. Comparative biochemistry of hepatomas. IV. Isotope studies of glucose and fructose metabolism in liver tumors of different growth rates. *Cancer Res* 1963;23:995–1002.
12. Burk D, Woods M, Hunter J. On the significance of glycolysis for cancer growth, with special reference to Morris rat hepatomas. *J Natl Cancer Inst* 1967;38:839–863.
13. Gallagher BM, Fowler JS, Gutterson NI, et al. Metabolic trapping as a principal of radiopharmaceutical design: some factors responsible for the biodistribution of [^{18}F]2-deoxy-2-fluoro-D-glucose. *J Nucl Med* 1978;19:1154–1161.
14. Schnitzer JJ, Morrel EM, Colton CK, Smith KA, Stemerman MB. Absolute quantitative autoradiography for low concentrations of [^{125}I]-labeled proteins in arterial tissue. *J Histochem Cytochem* 1987;35:1439–1450.
15. Cory JG, Whitford TN. Ribonucleotide reductase and DNA synthesis in Ehrlich ascites tumor cells. *Cancer Res* 1972;32:1301–1306.
16. Tsuya A, Shigematsu A. Microautoradiography. In: Mizuhara V, ed. *Autoradiography*. Tokyo: Ishiyaku Shuppan; 1978:72–129.
17. Kubota R, Yamada S, Ishiwata K, et al. Cellular accumulation of ^{18}F-labelled boronophenylalanine depending on DNA synthesis and melanin incorporation: a double-tracer microautoradiographic study of B16 melanomas in vivo. *Br J Cancer* 1993;67:701–705.
18. Cleaver JE. Thymidine metabolism and cell kinetics. In: Neuberger A, Tatum EL, eds. *Frontiers of biology 6*. Amsterdam: North-Holland Publishing; 1967:15–69.
19. Kubota R, Yamada S, Ishiwata K, Kubota K, Ido T. Active melanogenesis in non-S phase melanocytes in B16 melanomas in vivo investigated by double-tracer microautoradiography with ^{18}F-fluorodopa and ^{3}H-thymidine. *Br J Cancer* 1992;66:614–618.
20. Vaupel P, Fortmeyer HP, Runkel S, Kallinowski F. Blood flow, oxygen consumption, and tissue oxygenation of human breast cancer xenografts in nude rats. *Cancer Res* 1987;47:3496–3503.
21. Wahl RL, Clavo A, Brown RS, Roessner J. 2-Fluoro-2-deoxy-D-glucose (FDG) uptake into human cancers cell lines in increased by hypoxia. *J Nucl Med* 1992;33:841.
22. Wahl RL, Clavo AC. Effects of hypoxia on cultured human tumor cell uptake of thymidine, L-methionine and FDG. *J Nucl Med* 1993;34:73P.
23. Brown RS, Fisher SJ, Wahl RL. Autoradiographic evaluation of the intratumoral distribution of 2-deoxy-D-glucose and monoclonal antibodies in xenografts of human ovarian adenocarcinoma. *J Nucl Med* 1993;34:75–82.
24. Haberkorn U, Strauss LG, Dimitrak opoulou A, et al. PET studies of fluorodeoxyglucose metabolism in patients with recurrent colorectal tumors receiving radiotherapy. *J Nucl Med* 1991;32:1485–1490.
25. Higashi K, Clavo AC, Wahl RL. In vitro assessment of 2-fluoro-2-deoxy-D-glucose, L-methionine and thymidine as agents to monitor the early response of a human adenocarcinoma cell line to radiotherapy. *J Nucl Med* 1993;34:773–779.
26. Rozental JM, Levine RL, Mehta MP, et al. Early changes in tumor metabolism after treatment: the effects of stereotactic radiotherapy. *Int J Radiat Oncol Biol Phys* 1991;20:1053–1060.
27. Rozental JM, Levine RL, Nickles RJ, Dobkin JA. Glucose uptake in gliomas after treatment: a positron emission tomographic study. *Arch Neurol* 1989;46:1302–1307.
28. Rajs J, Harm T. Isolated rat cardiac myocytes as an experimental tool in the study of anoxic cell injury. Effect of reoxygenation—a preliminary report. *Forensic Sci Int* 1980;16:185–190.
29. Rajs J, Sundberg M, Harm T, Grandinsson M, Soderlund U. Interrelationships between ATP levels, enzyme leakage, gluconate uptake, trypan blue exclusion and length/width ratio of isolated rat cardiac myocytes subjected to anoxia and reoxygenation. *J Mol Cell Cardiol* 1980;12:1227–1238.
30. Yaoita H, Fischman AJ, Wilkinson R, et al. Distribution of deoxyglucose

and technetium-99m-glucarate in the acutely ischemic myocardium. *J Nucl Med* 1993;34:1303–1308.
31. Ames A 3rd, Nesbett FB. Pathophysiology of ischemic cell death: I. Time of onset of irreversible damage; importance of the different components of the ischemic insult. *Stroke* 1983;14:219–226.
32. Minn H, Kangas L, Knuutila V, Paul R, Sipila H. Determination of 2-fluoro-2-deoxy-D-glucose uptake and ATP level for evaluating drug effects in neoplastic cells. *Res Exp Med (Berl)* 1991;191:27–35.
33. Orrenius S, Thor H, Rajs J, Berggren M. Isolated rat hepatocytes as an experimental tool in the study of cell injury. Effect of anoxia. *Forensic Sci* 1976;8:255–263.
34. Espinoza MI, Parer JT. Mechanisms of asphyxial brain damage, and possible pharmacologic interventions, in the fetus. *Am J Obstet Gynecol* 1991; 164:1582–1591.
35. Montgomery POB, Karney D, Reynolds RC. Cellular and subcellular effects of ionizing radiations. *Am J Pathol* 1963;44:727–737.
36. Frank A, Gupta N. In vivo assessment of FDG, methionine and thymidine uptake (Letter). *J Nucl Med* 1993;34:2278–2279.
37. Shields AF, Lim K, Grierson J, Link J, Krohn KA. Utilization of labeled thymidine in DNA synthesis: studies for PET. *J Nucl Med* 1990;31:337–342.
38. Shields AF, Graham MM, Kozawa SM, et al. Contribution of labeled carbon dioxide to PET imaging of carbon-11-labeled compounds. *J Nucl Med* 1992;33:581–584.
39. Shields AF, Conti PS, Best MA. Clinical PET: neoplasms, CNS tumors, economics. In: *Continuing education lectures CEL 244*. New York: Society of Nuclear Medicine; 1992.
40. Higashi K, Clavo AC, Wahl RL. Does FDG uptake measure proliferative activity of human cancer cells? In vitro comparison with DNA flow cytometry and tritiated thymidine uptake. *J Nucl Med* 1993;34:414–419.
41. Weber G. Enzymology of cancer cells. *N Engl J Med* 1977;296:541–551.
42. Swann MM. The control of cell division: a review. *Cancer Res* 1957;17: 727–757.
43. Zotin AI. Rate of glucose oxidation in sea urchin eggs. *Nature* 1967;213: 529–530.
44. Pardee AB, Dubrow R, Hamlin JL, Kletzien RF. Animal cell cycle. *Ann Rev Biochem* 1978;47:715–750.
45. Cochran BH. The molecular action of platelet-derived growth factor. *Adv Cancer Res* 1985;45:183–216.
46. Brand K, Aichinger S, Forster S, et al. Cell-cycle-related metabolic and enzymatic events in proliferating rat thymocytes. *Eur J Biochem* 1988;172: 695–702.
47. Gossla R, Hartmann W, Heit W, Gaedicke G, Vetter U. Role of insulin during cell cycle in a myeloid cell line. *Leukemia* 1990;4:111–116.
48. Murray AW, Kirschner MW. Dominoes and clocks: the union of two views of the cell cycle. *Science* 1989;246:614–621.